Netsu Sokutei **27** (1) 19-29

解　説

Calorimetric Determination of the Number of Differently Bound Water Molecules in Phospholipid Bilayer Systems

Michiko Kodama and Hiroyuki Aoki

(Received December 16, 1999 ; Accepted December 21, 1999)

The present study has reviewed (i) how to classify the water molecules in multilamellar dispersions of lipid-water system on the basis of the ice-melting behavior as revealed by heating differential scanning calorimetry (DSC) and (ii) how to estimate the numbers of nonfreezable interlamellar and freezable interlamellar and bulk water molecules in this system from enthalpies of the ice-melting endotherms. Furthermore, by applying the calorimetric method, the numbers of the individual water molecules in different bonding modes were estimated for varying water contents of three lipid systems of different head groups (phosphatidylcholine, phosphatidylethanolamine and phosphatidylglycerol), and then used to construct water distribution diagrams of these systems. By comparing the resultant diagrams, the difference in the mode of hydration of three lipid bilayers, limited or infinite, was discussed.

1. Introduction

Phospholipids are major components of biomembranes and constitute a fundamental part of their bilayer structure. **Fig.1** represents a model structure of multilamellar bilayers in phospholipid-water system. Studies of water behavior in phospholipid bilayer systems are the subject of many investigations and have been performed by many techniques such as X-ray diffraction,[1-8] NMR spectroscopy [9-11] and differential scanning calorimetry (DSC).[12-24] DSC has been frequently used to investigate the bonding mode of water molecules to organic and inorganic substances. In this case, the thermal behavior associated with the melting of ice and sometimes with the freezing of water is measured. In this study, first, we discuss how the water molecules in phospholipid bilayer systems are classified by the ice-melting behavior (*i.e.*, the appearance of an endothermic peak related to the melting of ice) as revealed in the heating run of DSC. Next, we discuss how the number of water molecules in the different bonding modes is estimated from the ice-melting DSC curves.

2. Classification of Water Molecules in Lipid Bilayer Systems Based on Ice-Melting DSC Curves

2.1 Nonfreezable Interlamellar Water

A characteristic feature of DSC is its ability to distinguish clearly between freezable water (for which the ice-melting behavior is observed) and nonfreezable interlamellar water (for which it is not observed, even at temperatures low enough to form ice). As it is well known, the structure of ice is characterized by networks of hydrogen bonds formed among neighboring water molecules. Accordingly, it has been generally accepted that the water molecules present as nonfreezable water can not participate in the formation of such hydrogen bonds, even when cooled to extremely low temperatures. For the systems studied here, as is shown in **Fig.1**, water molecules, which exist in regions between adjacent lipid head groups in an intrabilayer [23] are considered to behave as nonfreezable water. This is because the

Department of Biochemistry, Okayama University of Science, Okayama 700-0005, Japan

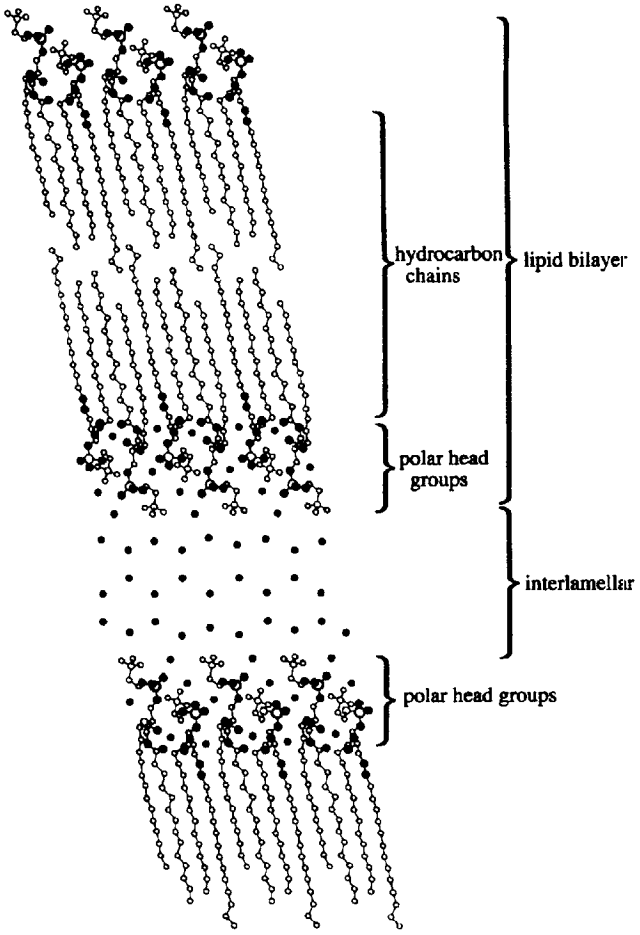

Fig.1 A model structure of multilamellar bilayers of a phospholipid-water system. A symbol of black circles shows oxygen atoms constituting H_2O and lipid molecules.

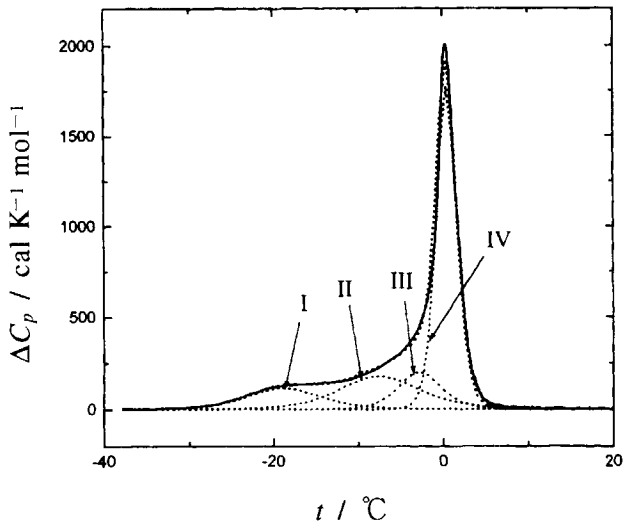

Fig.2 Examples of an ice-melting DSC curve (solid line) and its deconvolution analysis (dotted lines) in a lipid-water system. The apparent excess heat capacity (ΔC_p) is plotted as a function of temperature (t). The deconvoluted curves I, II and III are for the freezable interlamellar water and the deconvoluted curve IV is for the bulk water. The sum of the deconvoluted curves (the theoretical curve) is also shown by a dotted line.

water molecules, even in a liquid state, are confined within the narrow intrabilayer region as a result of their forming hydrogen bondings to carbonyl ester groups of the lipid. Also, water molecules that are bound to lipid head groups in an interbilayer region so tightly that they can not form hydrogen bonds with their neighboring water molecules, can be taken as nonfreezable water. However, if these water molecules have some freedom as required for the formation of water-water hydrogen bonds, the choice of being either freezable or nonfreezable water depends on the strength of the resultant hydrogen bonds. Thus, when the hydrogen bonds are weak, the energy necessary to break them is too small to be detected by DSC, so that the involved water molecules are counted as nonfreezable water. All the nonfreezable water in the systems studied in this investigation is found in regions between lamellae, and so is designated as nonfreezable interlamellar water.

2.2 Freezable Interlamellar Water and Bulk Water

On the other hand, the freezable water is present in two types. One exists in the interbilayer region [23] (see **Fig.1**), but it keeps the degree of freedom for its molecules at least to reorient themselves in order to form the ice-like hydrogen bonds. This water is designated as freezable interlamellar one. The other exists outside the bilayers and is designated as bulk water. However, the structure of ice derived from freezable interlamellar water is presumed to be far from that of hexagonal ice, while ice derived from bulk water is close to the most ordered hexagonal ice. The above discussed structural difference in the ice, although based upon some assumptions, is reflected in its melting behavior shown by a solid line in **Fig.2**. Thus, the ice obtained from freezable interlamellar water begins to melt at temperatures as low as $-45 \sim -35$ ℃ and continues to melt up to ca. 0 ℃. In contrast, the ice derived from bulk water melts in a narrow temperature range around 0 ℃. The ice-melting behavior observed over the wide temperature range below 0 ℃ suggests that the mode of hydrogen bonding in the

ice of the freezable interlamellar water molecules changes continuously in a way such as approaching more closely that of hexagonal ice, as the water molecules are more remote from the bilayer surfaces.

3. Estimation of the Number of Differently Bound Water Molecules Based on a Deconvolution Analysis of Ice-Melting DSC Curves

3.1 Definitions

As is discussed above, the water molecules in lipid-water systems are classified into three types: nonfreezable interlamellar-, freezable interlamellar- and bulk water. A correlation between the numbers of water molecules of these three types at a desired total water content is given by the following equation:

$$N_T = N_{I(nf)} + N_{I(f)} + N_B \qquad (1)$$

where N_T is the total number of water molecules per lipid molecule and $N_{I(nf)}$, $N_{I(f)}$ and N_B are the numbers per lipid molecule of nonfreezable interlamellar, freezable interlamellar and bulk water molecules, respectively. N_T is estimated from the amount of water added to a sample. When a molar mass is used, N_T is the sum of the molar numbers (per mol of lipid) of the three types of water and is equal to the water/lipid molar ratio, N_w, for samples of varying water contents. In the present study, N_T and N_w are treated separately. By using the known melting enthalpy of hexagonal ice, 1.436 kcal per mol of water, Eq.1 is replaced by

$$1.436\ (N_T - N_B) = 1.436\ (N_{I(nf)} + N_{I(f)}) \qquad (2)$$

In Eq.2, each term of $1.436 \times N$ is expressed in kcal per mol of lipid. Here, we assume that bulk water in the systems studied here behaves as free water. On this basis, the first term, $1.436N_T$, represents the melting enthalpy, ΔH_T, for N_T moles of all water added to 1 mole of lipid, by assuming that the water is all present as bulk water, and hence is a theoretical value. In addition, the second term, $1.436N_B$, corresponds to the melting enthalpy, ΔH_B, for N_B moles of water actually present as bulk water per 1 mole of lipid, and is experimentally determined from the ice-melting DSC curve. However, although it is needless to say for the first term on the right side of Eq.2, the second term on this side is not also comparable to the ice-melting enthalpy for $N_{I(f)}$ moles of freezable interlamellar water because its molar enthalpy

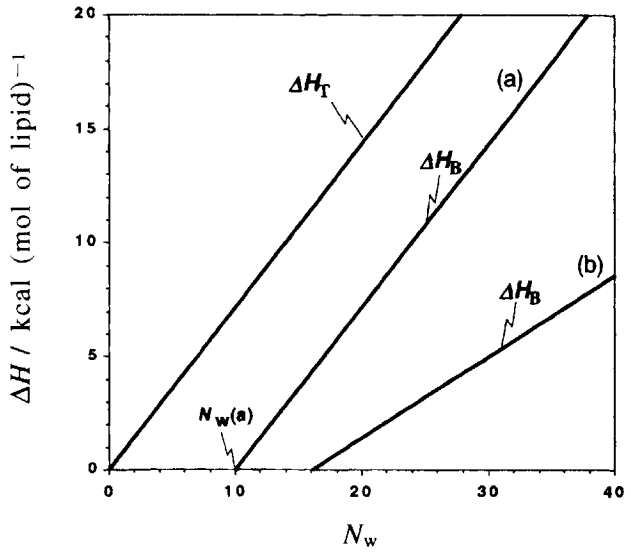

Fig.3 Comparison of ice-melting enthalpy curves of ΔH_B and ΔH_T for bulk water per mol of lipid. The ΔH_B curve is an experimental one determined by DSC and the ΔH_T curve is a theoretical one obtained by assuming that all the water added is present as free water. In this figure, the ΔH_B curve consists of the curves (a) and (b) for limited and infinite hydrations, respectively. N_w is a water/lipid molar ratio. $N_w(a)$ is the water/lipid molar ratio where the maximum amount of interlamellar water is reached in a lipid-water system.

is smaller than1.436 kcal mol^{-1} as will be discussed in the text. So, Eq.2 may be rewritten as

$$\Delta H_T - \Delta H_B = 1.436\ (N_{I(nf)} + N_{I(f)}) \qquad (3)$$

On the other hand, the above equations are limited to a certain water content of a lipid-water system. So, a more detailed picture is shown in **Fig.3** which takes into account the variation in water content. In this figure, the theoretical (ΔH_T) and experimental (ΔH_B) ice-melting enthalpies for the bulk water given in Eq.3 are plotted against N_w and are compared. Furthermore, the ΔH_B curve is compared in two typical cases designated by (a) - limited hydration - and (b) - infinite hydration. The noticeable points in **Fig.**3 are that (i) the bulk water appears for the first time at the N_w value where the ΔH_B curve intersects the abscissa and N_B at each N_w is calculated from $\Delta H_B/1.436$; (ii) the enthalpy difference, $\Delta H_T - \Delta H_B$, between the theoretical and experimental curves corresponds to $1.436N_I$, where N_I(= $N_{I(nf)}+N_{I(f)}$) in Eq.3, and so N_I at each N_w is calculated

from $(\Delta H_T - \Delta H_B)/1.436$. The ΔH_B curve (a) is parallel to the theoretical curve, indicating that the amount of the total (nonfreezable plus freezable) interlamellar water reaches a maximum at the N_w value of the intersection point, denoted as $N_w(a)$, and so $N_w(a)$ just gives the maximum amount of interlamellar water: above $N_w(a)$, all the water added exists as bulk water outside the lamellae. Thus, such a parallel curve proves a limited uptake of the interlamellar water. On the other hand, the ΔH_B curve (b), which is not parallel to the theoretical curve, indicates an infinite uptake of the interlamellar water. Thus, some of the water added beyond the intersection point exists as bulk water and the remainder increases the amount of the interlamellar water.

3.2 Deconvolution Analysis [18-22]

As discussed above, N_B and N_I are estimated from the enthalpy ΔH_B which is experimentally determined from the ice-melting DSC curve. So, it is understandable that ΔH_B is a chief determinant in the accuracy of the present method. From this viewpoint, to determine ΔH_B as accurately as possible, a deconvolution analysis was used to separate the ice-melting DSC curve into two components (or peaks), broad and sharp, for the freezable interlamellar and bulk water, respectively, because both components overlap at their basis. Furthermore, the broad component was deconvoluted into multiple components. The purpose is not only to improve the accuracy of the deconvolution analysis, but also to estimate $N_{I(nf)}$ and $N_{I(f)}$ given in Eq.3.

The deconvolution was performed according to a computer program for a multiple Gaussian curve analysis. An example of the deconvolution analysis is shown by dotted lines in **Fig.2**. In the present deconvolution, the ice-melting DSC curve was deconvoluted into the minimum number of components, by applying the following conditions that (i) the theoretical curve given by the sum of individual deconvoluted curves is best fitted to the experimental DSC curve; and (ii) both the half-height width and the midpoint temperature of each deconvoluted curve are maintained almost constant throughout all the deconvolutions for varying water contents. The standard deviations of the present deconvolutions are ca. 0.1 - 0.3 kcal K^{-1} mol^{-1}.

3.3 Estimation of the Number of Differently Bound Water Molecules

In **Fig.2**, deconvoluted curves are compared with the experimental DSC curve. The deconvoluted curve IV is for the bulk water and the deconvoluted curves I, II and III are for the freezable interlamellar water. Therefore, the melting enthalpy of the deconvoluted curve IV, ΔH_{IV}, gives the enthalpy ΔH_B in Eq.3, and so it was used to estimate N_I from $(\Delta H_T - \Delta H_B)/1.436$ discussed above. In **Fig.4**, the ice-melting enthalpy for the freezable interlamellar water, denoted as $\Delta H_{I(f)}$, which is given by the sum of the individual melting enthalpies of the deconvoluted curves I, II and III, is plotted against N_w and is compared with the ΔH_T and ΔH_B (a) curves shown in **Fig.3**. The $\Delta H_{I(f)}$ curve intersects the abscissa at the N_w value denoted as $N_w(b)$, above which freezable interlamellar water appears. Therefore, for $N_w \leq N_w(b)$ (I), all the water added is present as nonfreezable

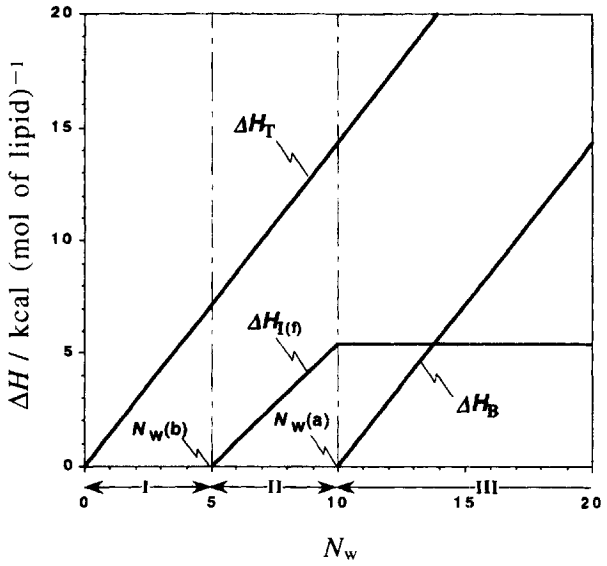

Fig.4 Comparison of ice-melting enthalpy curves of ΔH_B and $\Delta H_{I(f)}$ for bulk and freezable interlamellar water per mol of lipid. The ΔH_B and $\Delta H_{I(f)}$ curves are determined from the deconvoluted ice-melting curves for the bulk and freezable interlamellar water, respectively. $N_w(a)$ and $N_w(b)$ are the water/lipid molar ratios at the maximum amounts of the freezable and nonfreezable interlamellar water, respectively. The designations I, II and III represent three regions of $N_w \leq N_w(b)$ (*i.e.*, in the presence of only the nonfreezable interlamellar water), $N_w(b) < N_w \leq N_w(a)$ (*i.e.*, in the presence of the nonfreezable- and freezable-interlamellar water) and $N_w > N_w(a)$ (*i.e.*, in the presence of the nonfreezable- and freezable-interlamellar and bulk water), respectively.

Table 1 A summary in estimations of the number of differently bound water molecules for three water content regions (I, II and III) in the gel phase of the DPPC-water system.

	I	II	III
	N_w [2] $\leq N_w(b)$ [3]	$N_w(b) < N_w \leq N_w(a)$ [4]	$N_w > N_w(a)$
$N_{I(nf)}$ [1]	N_w	$N_w(b)$	$N_w(b)$
$N_{I(f)}$ [1]	0	$N_w - N_w(b)$	$(\Delta H_T - \Delta H_B)/1.436 - N_w(b)$
N_B [1]	0	0	$\Delta H_B/1.436$

1) $N_{I(nf)}$, $N_{I(f)}$ and N_B are the numbers (per lipid molecule) of nonfreezable interlamellar, freezable interlamellar and bulk water molecules.
2) N_w is a water/lipid molar ratio for samples of varying water contents.
3) $N_w(b)$ is the N_w value where the amount of nonfreezable interlamellar water reaches a maximum (see Fig.4).
4) $N_w(a)$ is the N_w value where the amount of the total (nonfreezable plus freezable) interlamellar water reaches a maximum (see Fig.4).

interlamellar water, and so $N_{I(nf)}$ at each N_w is equal to N_w. Here, if we assume a limited uptake of the nonfreezable interlamellar water, then $N_w(b)$ gives the maximum number of the nonfreezable interlamellar water molecules. This assumption seems to be reasonable because the van der Waals interaction force operating between the lipid hydrocarbon tails restricts an expansion of their head groups, [25, 26] resulting in a limited space for the intrabilayer regions. Accordingly, the maximum value of $N_{I(nf)}$ is equal to $N_w(b)$. For $N_w(b) < N_w \leq N_w(a)$ (II), *i.e.*, in the absence of bulk water, $N_{I(f)}$ at each N_w is calculated by subtracting $N_w(b)$ from N_w. For $N_w > N_w(a)$ (III), *i.e.*, in the presence of bulk water, $N_{I(f)}$ is obtained by subtracting $N_w(b)$ from the N_I value calculated from $(\Delta H_T - \Delta H_B)$ / 1.436 at each N_w. The estimations of $N_{I(nf)}$, $N_{I(f)}$ and N_B for varying water contents are summarized in **Table 1**.

3.4 Water-Distribution Diagrams

Values of $N_{I(nf)}$, $N_{I(f)}$ and N_B obtained according to the above calculations were used to construct a water distribution diagram for a limited hydration of a lipid-water system (**Fig.5**), where a cumulative number ($= N_{I(nf)} + N_{I(f)} + N_B$) per mol of lipid is plotted against N_w. The diagram provides much information such as (i) the number of water molecules in different binding modes at each N_w; (ii) the mode, whether limited or infinite, for the uptake of the water molecules; and (iii) the N_w value, at which the system is fully hydrated.

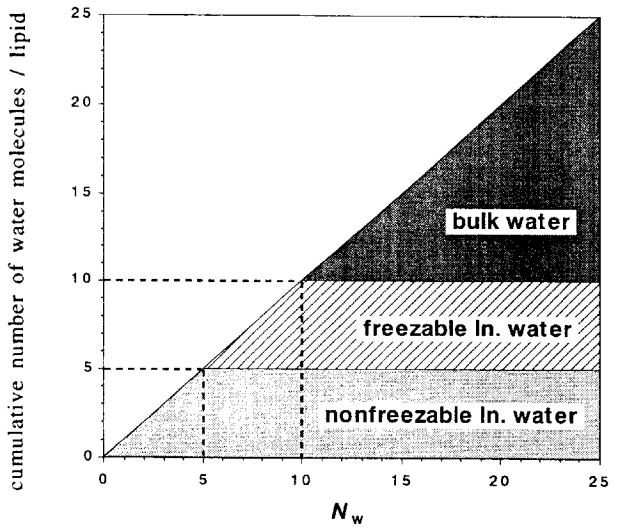

Fig.5 Water distribution diagram for a limited hydration of a lipid-water system. A cumulative number of water molecules (per lipid) in different bonding modes is plotted against the water/lipid molar ratio (N_w).

4. Experimental Techniques

The water distribution diagram shown in **Fig.5** was composed of the results of at least thirty samples of a lipid-water mixture containing from 0 to at least 40 wt % of water. The value of N_T in Eq.2, determined by weighing both the lipid and water, is also a dominant factor in the accuracy of the present method, similarly to the value of ΔH_B discussed above. From this viewpoint, samples of varying water contents were prepared in the

present study by successive additions of the desired amounts of water to the same dehydrated lipid. Thus, only the weight of water was changed throughout the preparation of a series of samples. The dehydrated lipid was prepared as follow: a lipid (approximately 30 mg) in a high-pressure crucible cell was dehydrated under high vacuum (10^{-4} Pa) at room temperature for at least 3 days until no mass loss was detected by electroanalysis. The crucible cell containing the dehydrated lipid was sealed off in a dry box filled with dry N_2 gas and then weighed by a microbalance. All the samples were weighed after adding the desired amounts of water and annealed by repeating thermal cycling at temperatures above and below the lipid phase transition until the same transition behavior was attained. After the annealing, the loss of water in the samples was checked by the microbalance.[13, 21]

5. Analysis of Water Molecules in the Gel Phase of Phospholipid-Water Systems

Phospholipids used in the present study are dipalmitoylphosphatidylcholine (DPPC) and dimyristoylphosphatidylethanolamine (DMPE) as neutral lipids, and dipalmitoylphosphatidylglycerol (DPPG) as an acidic lipid. The polar head groups of these lipids are compared in **Fig.6**.[27-30] It is worthy to note that these head groups provide many binding sites for a water molecule on the surface of a bilayer. PC and PE constitute the majority of the total phospholipids in biomembranes and are present as dipolar zwitterions at neutral pH. PG is a ubiquitous phospholipid in mitochondrial and chloroplast membranes and is negatively charged at neutral pH.[31] Since these lipids have charged groups, electrostatic forces operate not only between adjacent head groups in an intrabilayer (intermolecular force), but also between adjacent bilayers (inter-surface force), although the forces are opposite in sign or direction for the neutral and acidic lipids. Furthermore, results of X-ray crystallographic studies previously reported by other workers should be mentioned here. Thus, two adjacent PC molecules in an intrabilayer are linked to each other via a water-based hydrogen bond.[28,32] However, PE molecules in an intrabilayer interact directly via a hydrogen bond formed between the amino group of one molecule and the phosphate group of an adjacent molecule.[28,29,32] For PG used in Na^+-PG, the counterions are present in a

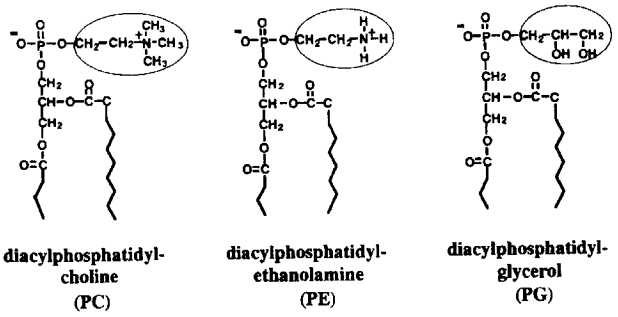

Fig.6 Difference in the polar head groups of phosphatidylcholine (PC), phosphatidylethanolamine (PE) and phosphatidylglycerol (PG).

layer sandwiched by the head groups of adjacent bilayers.[33]

On the other hand, lipid-water systems are mostly present in either a gel or a liquid crystal phase depending on temperature. If the ice-melting DSC peak (whether broad or sharp) is successively followed by the gel-to-liquid crystal phase transition, the melting behavior is known to be derived from the water molecules of the gel phase. If no phase transition is observed at a temperature higher than that of the ice-melting, then the ice is assigned to one of the liquid crystal phase. In this connection, all the ice-melting peaks of the present three systems are observed to be followed by the gel-to-liquid crystal phase transitions unless thermal annealing treatments are adopted for these samples.[14-16, 18-20, 34, 35] On this basis, we measured the ice-melting behavior of the gel phases of three systems and constructed the water distribution diagrams of these gel phases, particularly with a view to answering the following question: Is there any difference between neutral and acidic phospholipids in the mode of incorporation of water molecules between their lamellae ?

Fig.7 shows a series of typical DSC curves for samples of the DPPC-water mixture with increasing water content expressed as {(g water) / (g lipid + g water) × 100} and designated as W_{H2O}. The ice-melting peaks are followed by two lipid transition peaks of the gel($L_{\beta'}$)-to-gel($P_{\beta'}$) and subsequent gel ($P_{\beta'}$)-to-liquid crystal phases, generally called the T_p and T_m transitions, respectively. In **Fig.8**, enlarged scale ice-melting peaks are compared to detail their broad components, particularly for W_{H2O} < 20 wt % where the water content is successively changed at short intervals of about one wt %. Although discussed

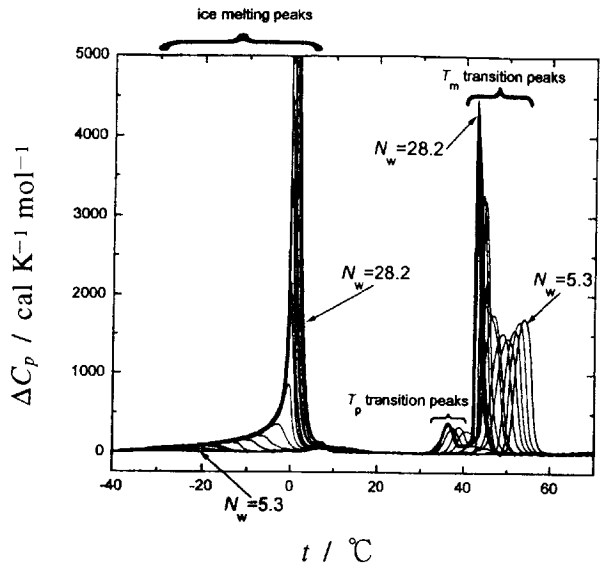

Fig.7 A series of DSC curves of the DPPC-water system ranging, in water content, from 11.5 (N_w = 5.3) to 40.9 wt % (N_w = 28.2).

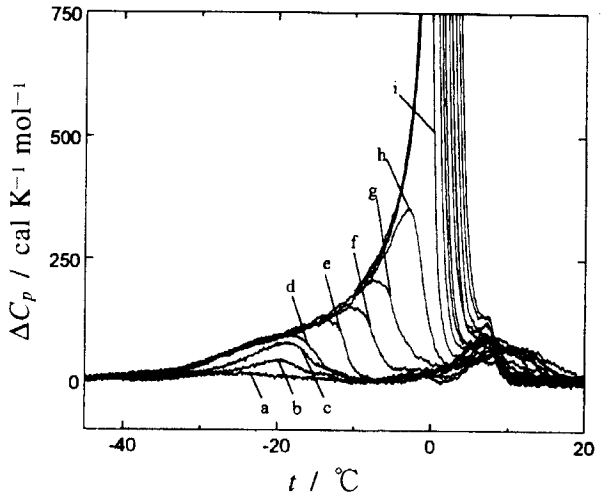

Fig.8 Variation of the broad component of ice-melting DSC curves with increasing water content for the gel phase of the DPPC-water system. Only low water contents are indicated in wt %: a-11.5(5.3); b-12.6(5.87); c-12.8(5.98); d-13.1(6.2); e-14.1(6.7); f-14.8(7.0); g-16.1(7.8); h-17.4(8.6); i-20.1(10.2). The numbers in parentheses show the corresponding N_w values.

later in the text, the freezable interlamellar water of the DPPC-water system is observed to appear at W_{H_2O} ~11 wt % (N_w ~5), therefore, N_w(b) ~5. However, the ice-melting behavior (curves a-c) for ~11 wt % (N_w ~5)< W_{H_2O} <~13 wt % (N_w ~6) is different from that (curves d-i) for W_{H_2O} >~13 wt %. Thus, for a very small amount of freezable interlamellar water (W_{H_2O} = 11.5 wt %, N_w = 5.3) (curve a), a broad, low, flat peak extending over a fairly wide temperature range is observed. Yet, even though the amount of the freezable interlamellar water is slightly less than one molecule of H_2O per lipid (W_{H_2O} = 12.8 wt %, N_w = 5.98) (curve c), the melting peak is broader and is not fitted to similar peaks observed for N_w >6. Such a broadening in no similar shapes is characteristic of freezable interlamellar water in amount of less than one molecule per lipid, namely, for 5 < N_w < 6. By assuming multiple binding sites to the water moleculs on the bilayer surface, it is suggested that 1 H_2O/lipid of freezable interlamellar water is not enough to cover all the binding sites. As a result, a localized growth of the water molecules into ice on cooling would occur on the bilayer surface, resulting in a broadening of the ice-melting peak. Therefore, one molecule of H_2O per lipid is a critical amount required for the freezable interlamellar water to form ice-like hydrogen bonds characterized by the ice-melting peaks in similar shapes. However, the freezable interlamellar water molecules above the critical amount (1H_2O/lipid) also interact with one another in different hydrogen bonding modes which become closer to that of free water with increasing water content.

According to the method discussed above, the ice-melting DSC peaks observed for N_w >6 (W_{H_2O} >13 wt %) are deconvoluted. In **Fig.9**, typical results of the deconvolution analysis are compared at different water contents of 16.1, 20.1 and 22.1 wt %. On the whole, the number of deconvoluted curves increases and the area of each curve becomes larger, with increasing water content. The broad peak for the freezable interlamellar water is shown to be finally deconvoluted into four curves, I, II, III and IV, which successively appear with increasing water content. A deconvoluted curve V for the bulk water is observed at water contents of 20.1 and 22.1 wt %. In **Fig.10**, the ice-melting enthalpies ΔH_I, ΔH_{II}, ΔH_{III} and ΔH_{IV} of the respective deconvoluted curves I, II, III and IV are plotted against N_w, together with the sum of these enthalpies, $\Delta H_{I(f)}$. In **Fig.11**, the ice-melting enthalpy ΔH_V of the deconvoluted curve V, comparable to ΔH_B in Eq.3, is plotted against N_w and the ΔH_B (=ΔH_V) curve is compared with the $\Delta H_{I(f)}$ curve shown in **Fig.10**.

First, focusing on **Fig.10**, it is seen that with

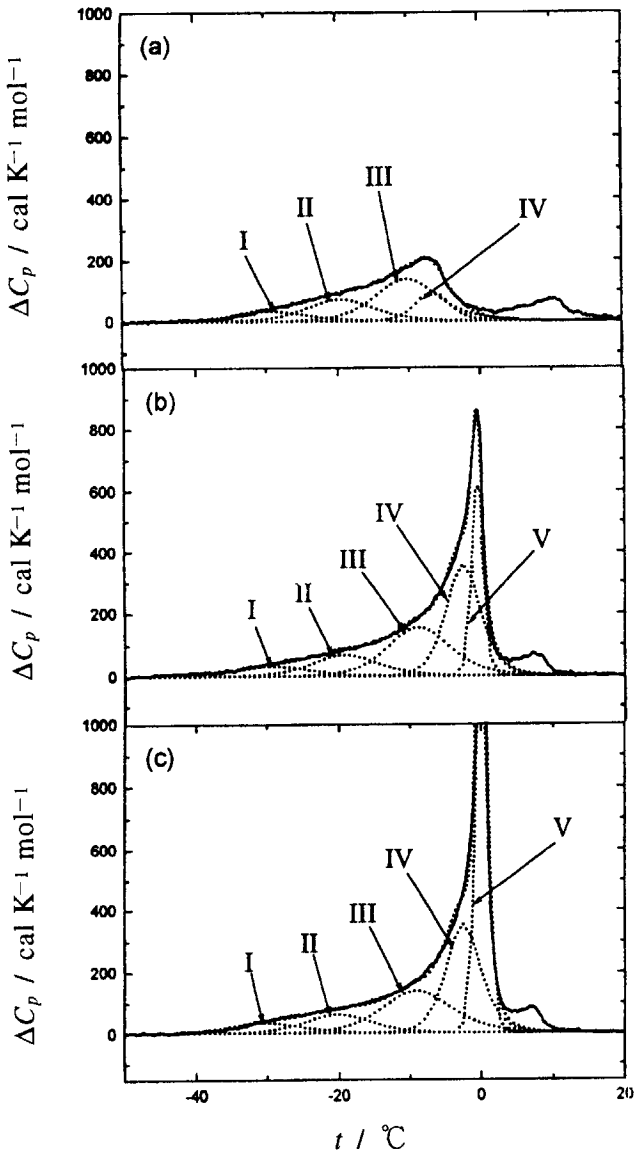

Fig.9 Deconvolution analysis of ice-melting DSC curves for the gel phase of the DPPC-water system. Water contents are given in wt %: a-16.1(7.8); b-20.1(10.2); c-22.1(11.6). The numbers in parentheses show the corresponding N_w values. The deconvoluted curves I - V and their sum (the theoretical curve) are shown by dotted lines and the DSC curves by solid lines.

increasing water content, the ΔH_I, ΔH_{II}, ΔH_{III} and ΔH_{IV} curves appear in this order and reach maxima in the same order. Every curve gently increases before arriving at a plateau, so that the $\Delta H_{I(f)}$ curve also shows the same behavior. Consequently, N_w (~15) at the beginning of the plateau of the $\Delta H_{I(f)}$ curve is higher than that (~10) predicted from the extrapolated (dotted) lines. On the other hand, the $\Delta H_{I(f)}$ curve intersects the abscissa at N_w ~5. Therefore, the limiting, maximum number

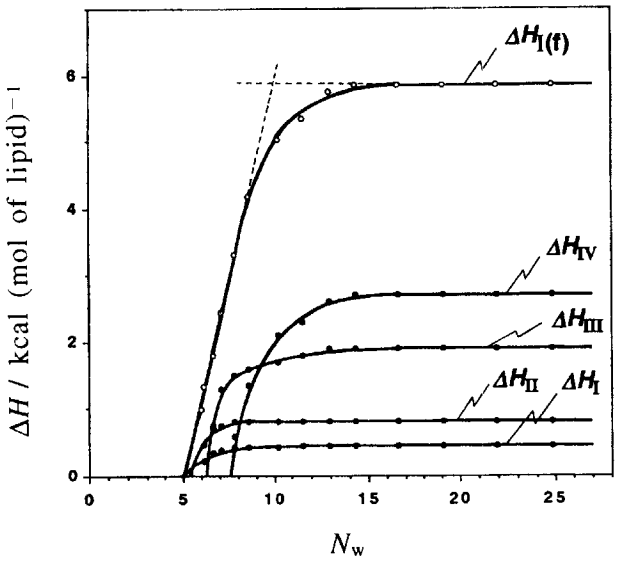

Fig.10 Plots of ice-melting enthalpies for the freezable interlamellar water against N_w in the gel phase of the DPPC-water system. ΔH_I, ΔH_{II}, ΔH_{III} and ΔH_{IV} show the individual enthalpies of the deconvoluted curves I, II, III and IV shown in Fig.9 and $\Delta H_{I(f)}$ shows the sum of these enthalpies.

of the nonfreezable interlamellar water molecules for the gel phase of the DPPC-water system is approximately 5 H_2O per lipid. Next, in **Fig.11**, the ΔH_B curve is also shown to increase gently up to N_w ~15, after which it increases linearly and in parallel to the theoretical ΔH_T line. Accordingly, the amount of the total interlamellar water is the same for water contents above the boundary N_w (~15), indicating the appearance of a fully hydrated gel phase. In this case, the maximum amount of the total interlamellar water can be determined graphically by extrapolating the linear ΔH_B curve to N_w below 15. Thus, N_w of the intersection point just corresponds to the maximum number of interlamellar water molecules, *i.e.*, 10 H_2O per lipid for the DPPC-water system.

Furthermore, it is seen from **Fig.11** that the nonlinear increase for both the $\Delta H_{I(f)}$ and ΔH_B curves takes place in the same water content region of $8 < N_w < 15$. Accordingly, it is understandable that the deviations of the $\Delta H_{I(f)}$ curve from the extrapolated ideal (dotted) line is caused by the bulk water which appears although the limiting, maximum amount of interlamellar water is not yet reached (in other words, the gel phase is not fully hydrated). This indicates the existence of a specific region ($8 < N_w < 15$), taken as a

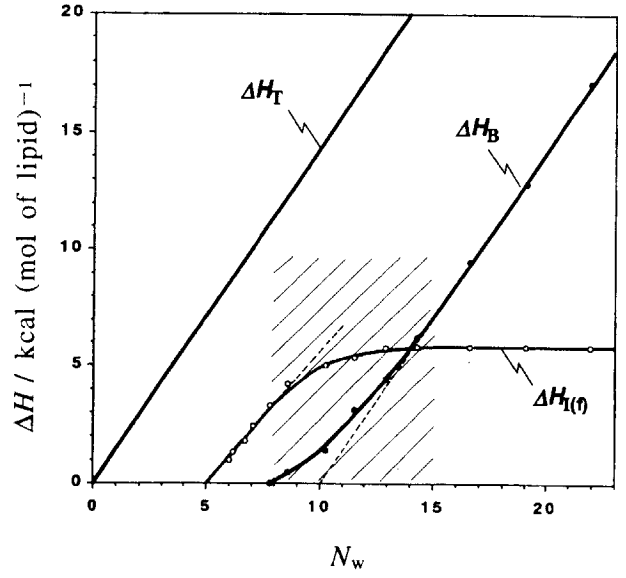

Fig.11 Comparison of ΔH_T, ΔH_B and $\Delta H_{I(f)}$ curves for the gel phase of the DPPC-water system. Hatched lines within range $8 < N_w < 15$ represent the pre-region (see text).

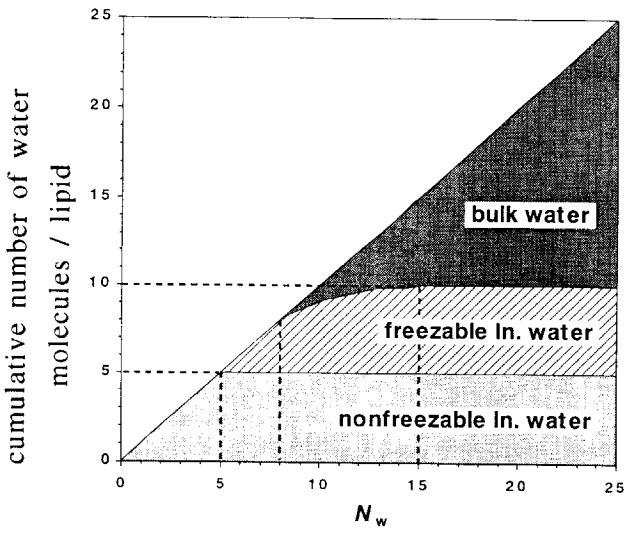

Fig.12 Water distribution diagram for the gel phase of the DPPC-water system. A cumulative number of water molecules (per lipid) present as nonfreezable and freezable interlamellar water and as bulk water is plotted against N_w.

pre-region,[6,8,9,21,22] and designated by hatched lines in **Fig.11**. In this region, the bulk water content likewise increases, little by little, until the maximum amount of the freezable interlamellar water is reached. Above this amount, all the added water is present as bulk water, so that the ΔH_B curve becomes parallel to the straight ΔH_T line.

Another point to notice in **Fig.11**, except the pre-region, is the difference in slope between the linear curves of $\Delta H_{I(f)}$ ($N_w < 8$) and ΔH_B ($N_w > 15$). Thus, although the $\Delta H_{I(f)}$ curve is also linear at N_w values below the pre-region, it is not parallel to the ΔH_T line and therefore, to the linear ΔH_B curve at N_w values above the pre-region. The slopes of the linear curves of ΔH_B and $\Delta H_{I(f)}$ are only characterized by the bulk and freezable interlamellar water, respectively, and so give individual molar ice-melting enthalpies for both types of water. On this basis, the individual average molar melting enthalpies for the bulk and freezable interlamellar water were estimated from the slopes of the respective straight ΔH_B and $\Delta H_{I(f)}$ lines obtained by a least-squares method. The average melting enthalpy for the bulk water is 1.420 kcal per mol of H_2O and it is very close to the known value estimated from the ΔH_T line. For the freezable interlamellar water, the estimated average melting enthalpy is 1.201 kcal per mol of H_2O and it is smaller than that for the bulk water. The above estimations evidence a difference in the molar ice-melting enthalpy between the freezable interlamellar and bulk water and this difference is related to different hydrogen-bond modes for both types of water.

The values of $N_{I(nf)}$, $N_{I(f)}$ and N_B for varying water contents were estimated according to the method discussed above. In **Fig.12**, the cumulative number of $N_{I(nf)}$, $N_{I(f)}$ and N_B is plotted against N_w. On the basis of the water distribution diagram, the following results are obtained for the gel phase of the DPPC-water system: (i) the limiting, maximum numbers of water molecules are approximately 5 H_2O and 5 ($= 10 - 5$) H_2O per lipid for the nonfreezable and freezable interlamellar water, respectively; (ii) these maximum values are reached at water/lipid molar ratios of approximately 5 and 15, respectively; and (iii) the pre-region exists in the range of $\sim 8 < N_w < \sim 15$, before the attainment of a full hydration of the gel phase.

Water distribution diagrams for respective gel phases of the DMPE-[21] and DPPG-water systems [22] were prepared according to the same method as that for the DPPC-water system and resultant diagrams are shown in **Figs.13** and **14**, respectively. For the DPPG-water system, the water content was continuously changed up to 90 wt % ($N_w = 374$) to investigate whether the hydration

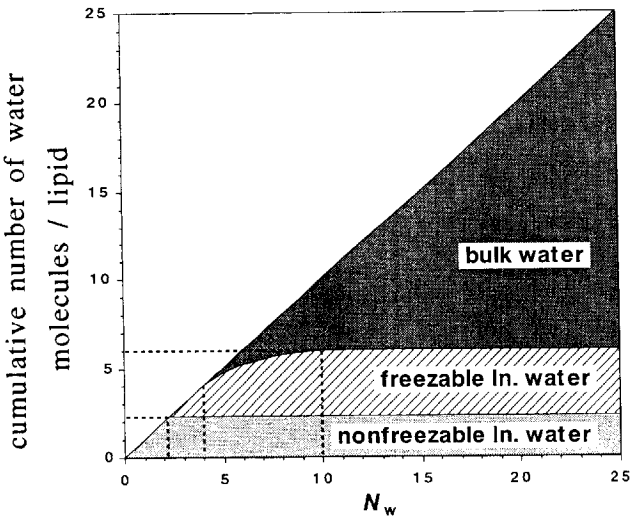

Fig.13 Water distribution diagram for the gel phase of the DMPE-water system. A cumulative number of water molecules (per lipid) present as nonfreezable and freezable interlamellar water and as bulk water is plotted against N_w.

is limited or infinite, and therefore, the water distribution diagram of this system is shown over the wide N_w range up to 400 (**Fig.14A**) and in an enlarged scale up to $N_w = 50$ (**Fig.14B**).

In **Fig.13**, a limited hydration is also observed for the DMPE-water system. For a fully hydrated gel phase of this system, the amount of interlamellar water is approximately 6 H_2O per lipid which comes from 2.3 nonfreezable interlamellar water molecules plus 3.7 freezable interlamellar water molecules, indicating a smaller amount of interlamellar water, compared with that for the fully hydrated DPPC gel phase shown in **Fig.12**. For the difference in the amount of interlamellar water, a point to be considered is an intrabilayer space between adjacent head groups which is narrower for DMPE bilayers than for DPPC ones because a geometrical size of these head groups is smaller for the former than for the latter. An additional noticeable point is the difference in intermolecular interactions of these head groups, as discussed above. Thus, adjacent head groups of DMPE bind directly via their intermolecular hydrogen bonds, in contrast to adjacent DPPC head groups which are linked via water-based hydrogen bonds.

On the other hand, the water distribution diagram in **Fig.14** shows an infinite incorporation of freezable interlamellar water, *i.e.*, an infinite hydration of DPPG

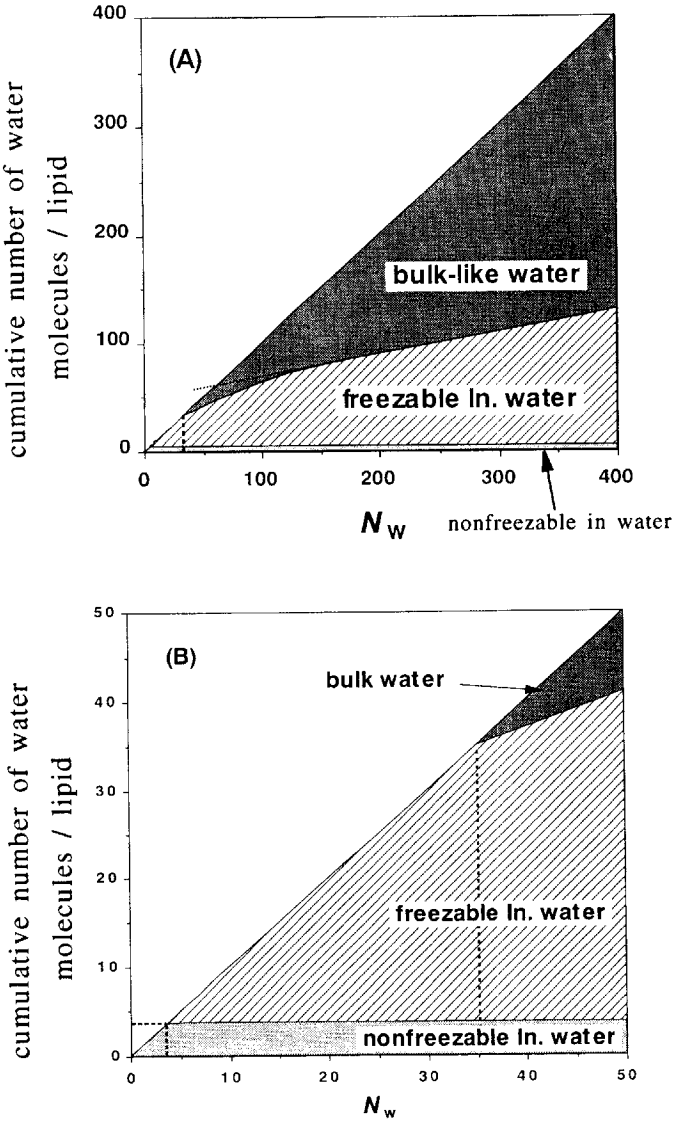

Fig.14 Water distribution diagram up to (A) N_w = 400 and (B) N_w = 50 for the gel phase of the DPPG-water system. A cumulative number of water molecules (per lipid) present as nonfreezable and freezable interlamellar water and as bulk water is plotted against N_w.

bilayers. Repulsion forces operate between apposing DPPG bilayer surfaces. The inter-surface forces cause the infinite incorporation of water molecules between DPPG bilayers, in contrast with the limited hydration of the neutral lipid bilayers shown in **Figs.12** and **13**.

References

1) M. J. Ruocco and G. Shipley, *Biochim. Biophys. Acta* **691**, 309 (1982).
2) T. J. McIntosh and S. A. Simon, *Biochemistry* **25**, 4058 (1986).

3) T. J. McIntosh and S. A. Simon, *Biochemistry* **25**, 4948 (1986).
4) J. M. Seddon, G. Cevc, R. D. Kayer, and D. Marsh, *Biochemistry* **23**, 2634 (1984).
5) R. P. Rand and V. A. Parsegian, *Biochim. Biophys. Acta* **988**, 351 (1989).
6) G. Klose, B. König, H. W. Meyer, G. Schulze, and G. Degovics, *Chem. Phys. Lipids* **47**, 225 (1988).
7) M. C. Wiener, R. M. Suter, and J. F. Nagle, *Biophys. J.* **55**, 315 (1989).
8) J. F. Nagle, R. Zhang, T. Stephanie-Nagle, W. Sun, H. I. Petrache, and R. M. Suter, *Biophys. J.* **70**, 1419 (1996).
9) K. Gawrisch, W. Richter, A. Möps, P. Balgavy, K. Arnold, and G. Klose, *Studia Biophys.* **108**, 5 (1985).
10) J. Ulmius, H. Wennerström, G. Lindblom, and G. Arvidson, *Biochemistry* **16**, 5742 (1977).
11) E. G. Finer and A. Darke, *Chem. Phys. Lipids* **12**, 1 (1974).
12) D. Chapman, R. M. Williams, and B. D. Ladbrooke, *Chem. Phys. Lipids* **1**, 445 (1967).
13) M. Kodama, M. Kuwabara, and S. Seki, *Thermochim. Acta* **50**, 81 (1981).
14) M. Kodama, H. Hashigami, and S. Seki, *Thermochim. Acta* **88**, 217 (1985).
15) M. Kodama, *Thermochim. Acta* **109**, 81 (1986).
16) M. Kodama, H. Hashigami, and S. Seki, *J. Colloid Interface Sci.* **117**, 497 (1987).
17) M. Kodama and S. Seki, *Adv. Colloid Interface Sci.* **35**, 1 (1991).
18) M. Kodama, H. Inoue, and Y. Tsuchida, *Thermochim. Acta* **266**, 373 (1995).
19) H. Aoki and M. Kodama, *J. Thermal Anal.* **49**, 839 (1997).
20) H. Takahashi, H. Aoki, H. Inoue, M. Kodama, and I. Hatta, *Thermochim. Acta* **303**, 93 (1997).
21) M. Kodama, H. Aoki, H. Takahashi and I. Hatta, *Biochim. Biophys. Acta* **1329**, 61 (1997).
22) M. Kodama, J. Nakamura, T. Miyata and H. Aoki, *J. Thermal. Anal.* **51**, 91 (1998).
23) J. F. Nagle and M. C. Wiener, *Biochim. Biophys. Acta* **942**, 1 (1988).
24) S. C. Chen, J. M. Sturtevent and B. J. Gaffeny, *Proc. Natl. Acad. Sci. USA* **77**, 5060 (1980).
25) J. F. Nagle and D. A. Wilkinson, *Biophys. J.* **23**, 159 (1978).
26) D. A. Wilkinson and J. F. Nagle, *Biochemistry* **20**, 187 (1981).
27) R. Harrison and G.G. Lunt, Biological Membranes, 2nd edn., Blackie and Son Ltd., London, 1980, p. 68.
28) G. G. Shipley, in D. M. Small (Ed.), Handbook of Lipid Research, Vol.4, Plenum Press, New York, 1986, p. 97.
29) J. M. Boggs, *Biochim. Biophys. Acta* **906**, 353 (1987).
30) M. Kodama and T. Miyata, *Colloid Surfaces A* **109**, 283 (1996).
31) M. Kodama and T. Miyata, *Thermochim. Acta* **267**, 365 (1995).
32) H. Hauser, I. Pascher, R. H. Pearson, and S. Sundell, *Biochim. Biophys. Acta* **650**, 21 (1981).
33) I. Pascher, S. Sundell, K. Harlos, and H. Eibl, *Biochim. Biophys. Acta* **896**, 77 (1987).
34) M. Kodama, T. Miyata, and T. Yokoyama, *Biochim. Biophys. Acta* **1168**, 243 (1993).
35) M. Kodama, H. Aoki, and T. Miyata, *Biophys. Chem.* **79**, 205 (1999).

要　旨

本研究では，リン脂質2分子膜の水和現象に着目して，次の2点をまず，解説する。：(i) 昇温示差走査熱量測定（DSC）によって観測される氷融解挙動から，脂質−水の多重膜分散系の水分子がどのように分類されるか，(ii) 氷融解に基づくエンタルピーから，この系の不凍結層間，凍結層間およびバルク水分子の数はどのようにして見積られるか。さらに，その熱的手法を適用することで，親水頭部の異なる3種（フォスファチジルコリン，フォスファチジルエタノールアミン，フォスファチジルグリセロール）のリン脂質系での結合様式の異なる3種の水分子数の各々を見積り，これを基にして，水分率変化に対する水分布ダイアグラムを作製した。得られた3種系のダイアグラムを比較することで，これらリン脂質2分子膜の有限か無限かの水和様式の違いを議論した。